Journal of Hazardous Materials 188 (2011) 363–368

Contents lists available at ScienceDirect

Journal of Hazardous Materials

journal homepage: www.elsevier.com/locate/jhazmat

Template-free formation of vertically oriented TiO_2 nanorods with uniform distribution for organics-sensing application

Qinghui Mu [a], Yaogang Li [a], Qinghong Zhang [b,*], Hongzhi Wang [a,*]

[a] State Key Laboratory for Modification of Chemical Fibers and Polymer Maters Donghua University, Shanghai, 201620, PR China
[b] College of Materials Science and Engineering Donghua University, Shanghai, 201620, PR China

ARTICLE INFO

Article history:
Received 15 December 2010
Received in revised form 26 January 2011
Accepted 29 January 2011
Available online 4 February 2011

Keywords:
Nanorod
Titanium dioxide
Mixed crystal effect
Sensing
Photocurrent

ABSTRACT

High-density arrays of vertically oriented TiO_2 nanorods with uniform distribution on Ti foil have been formed through template-free oxidation of Ti in hydrogen peroxide solutions. Subsequent thermal treatment was applied for growing mixed crystal structures to pursue higher performance. Morphology characterization using field emission scanning electron microscopy (FESEM) shows a nanorod diameter in the range of 20–50 nm with a length of 1.5 μm. X-ray diffraction (XRD) measurement demonstrates the crystallization of the TiO_2 nanorods prior to thermal treatment and the formation of anatase and rutile mixed phase after thermal treatment. The mixed crystal TiO_2 nanorods show a much higher performance than pure anatase in photoelectrochemical experiments. Steady-state photocurrent resulted from photocatalytic oxidation of organic compounds by TiO_2 nanorods is employed as response signal in determination of the organics to yield a linear range of 0–1.1 mM for glucose. For other organics, an excellent linear relationship between the net steady-state photocurrent and the concentration of electrons transferred in exhaustive oxidation for these organics is obtained, which empowers the mixed crystal TiO_2 nanorods to serve as versatile material in organics-sensing application.

1. Introduction

Titanium dioxide is a versatile material and has been investigated considerably due to its unique photoelectronic and photochemical properties [1]. As photocatalyst for water splitting and degradation of organics, TiO_2 powder may have disadvantage in practical applications because of the difficulties in separating and recycling the fine particles [2]. TiO_2 nanocrystalline film which immobilizes the semiconductor catalyst on a solid support will exhibit its advantage in this regard. A number of methods have been developed to prepare TiO_2 thin films, for instance, electron-beam evaporation [3], chemical vapor deposition [4,5], physical vapor deposition [6], dip-coating [7,8], spin-coating [9], and screen-printing [10,11]. The thin films prepared through those methods are usually composed of TiO_2 nanoparticles, as illustrated in Fig. 1A. The photogenerated electrons transport across the nanoporous TiO_2 layer via the TiO_2 network formed by the interconnected nanoparticles. However, some of these particles may not be interconnected, which results in a limited number of effective electron pathways that have the shortest distance and lowest resistance [12]. Furthermore, the structural disorder at the contact between two crystalline nanoparticles leads to enhanced scattering of free electrons, thus reducing electron mobility [13]. Recently, the use of one-dimensional nanostructures instead of nanocrystalline films in photoelectrochemistry has been considered. TiO_2 nanorods [14], nanotubes [15,16], nanowires [17,18] and nanocolumns [19] have been used in highly efficient photovoltaic devices and as photocatalysts for hydrogen generation and degradation of organic pollutants. These one-dimensional nanomaterials with ordered architecture (Fig. 1B) allow for an oriented and much shorter random walk path for photogenerated carriers. As a result, improved charge separation and charge transport can be achieved [13].

The formation of one-dimensional nanostructures has been realized using various techniques. Anodization of Ti foil is now widely used to prepare TiO_2 nanotube arrays [15], but the corrosive etching process in the anodization takes place only when the toxic F^- is added. Although TiO_2 nanotubes and nanorods were also fabricated by templating ZnO nanorod array film through sol–gel process [20] and liquid phase deposition [21], the formation and subsequent removal of the ZnO template using wet-chemical etching complicated these methods. Template-free formation of one-dimensional TiO_2 nanorod arrays was achieved by oxidizing titanium substrate in an oxidation atmosphere at 850 °C [22,23]. Besides, fabrication of TiO_2 nanorod arrays on transparent conducting substrates was accomplished in solutions containing HCl without template [14,18,24]. However, the TiO_2 synthesized by

* Corresponding authors. Tel.: +86 21 67792881; fax: +86 21 67792855.
E-mail addresses: zhangqh@dhu.edu.cn (Q. Zhang), wanghz@dhu.edu.cn (H. Wang).

0304-3894/$ – see front matter © 2011 Elsevier B.V. All rights reserved.
doi:10.1016/j.jhazmat.2011.01.125

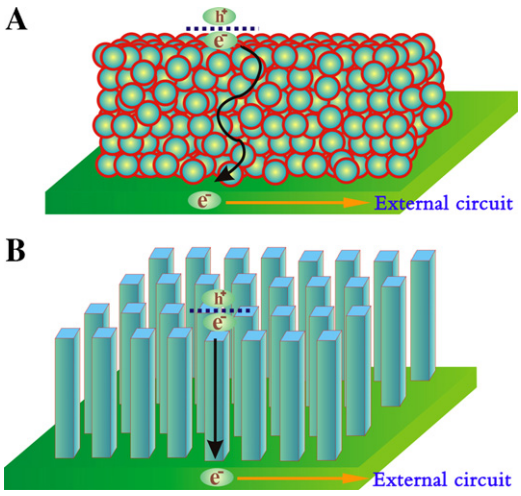

Fig. 1. Schematic diagrams of electron pathways in films composed of disordered nanoparticles and oriented nanoarrays.

the two above mentioned methods was rutile phase due to the high temperature and strong acidic medium applied during respective synthesis. Among the three different crystal structures of TiO_2, rutile, anatase, and brookite, rutile is the thermodynamically stable phase, whereas anatase has been generally accepted to have a higher photocatalytic activity than rutile owing to its anomalously large Born effective charge tensor as the result of the presence of enhanced Ti(3d states)-O(2p states) hybridization [25]. The photocatalytic activity of anatase TiO_2 can be greatly improved by mixing rutile nanostructures due to the mixed crystal effect [26,27]. Therefore, safe and simple formation of TiO_2 nanorod arrays with anatase or anatase/rutile structure is significant for their application in photovoltaic devices and photocatalysis.

In recent years, TiO_2 film composed of nanoparticles has been used as a sensor for water quality assessment based on the photocatalytic oxidation of organics [28]. Electrocatalysis of some novel electrodes, such as PbO_2 modified electrode [29], RhO_2/Ti electrode [30], copper electrode [31,32], boron-doped diamond electrode [33,34], have been used in determination of chemical oxygen demand (COD) based on the measurement of currents or charge generated from electrocatalytic oxidation of organic compounds. Photocatalytic oxidation approach, which utilizes TiO_2 as photocatalyst, can offer superior oxidation ability for oxidizing a much wider spectrum of organic compounds [35]. Therefore, there is a promising application for TiO_2 photocatalysis in determination of organics in aqueous solution by analyzing the photocurrents corresponded to the photocatalytic oxidation of the organics. However, the application of one-dimensional TiO_2 nanostructures in this field was seldom reported.

In this paper, a simple and undefiled method was introduced to fabricate large-scale, uniformly distributed and vertically oriented TiO_2 nanorod arrays on a titanium substrate using H_2O_2 solutions as the oxygen source in the oxidation of Ti at a low temperature. The prepared TiO_2 was in anatase phase and mixed phase after thermal treatment. The TiO_2 nanorod arrays with mixed phase were verified to have a higher photocatalytic activity, and were used as sensors to assemble photoelectrochemical cells for organics-sensing application in aqueous solutions.

2. Experimental

Formation and characterization of TiO_2 nanorod arrays: Ti foil (purity 99.99%) was purchased from Shanghai Zhenming nonferrous metal material Co., Ltd. The other chemicals were analytical grade and used as received from Sinopharm Chemical Reagent Co., Ltd. Ti foil sized 2 cm × 2 cm × 0.1 mm was degreased by sonication in acetone, 2-propanol, and ethanol to remove the contamination, subsequently rinsed with ultrapure water (18.2 MΩ), and finally dried in a nitrogen stream. After rinsing, Ti foil was soaked in a H_2O_2 solution (30 mL, 30 wt%). Then the solution was heated up to 80 °C, and kept at 80 °C for 72 h. Finally, the sample was taken out and rinsed with copious amounts of ultrapure water followed by thermal treatment in a muffle furnace at different temperature. Morphology of TiO_2 nanorod arrays was characterized by a field emission scanning electronic microscopy (FESEM, S-4800, Hitachi, Japan). The crystal structure of TiO_2 nanorods was investigated by an X-ray diffraction technique (XRD, D/max 2550 V, Rigaku, Japan) with Cu Kα (λ = 1.54 Å) radiation at 40 kV and 200 mA in 2θ ranging from 20° to 80°. The mass fraction of rutile (X_R) in the samples was calculated using the following equation [36]: $X_R = (1 + 0.8 I_A/I_R)^{-1}$, where I_A and I_R were the main intensities of anatase (1 0 1) peak and rutile (1 1 0) peak, respectively.

Photoelectrochemical measurements: Solutions needed in the whole experiment were prepared by dissolving the regents in ultrapure water (18.2 MΩ). All photoelectrochemical experiments were performed at room temperature in a three-electrode photoelectrochemical cell containing NaH_2PO_4 (1 M) solution with a quartz window for UV illumination. TiO_2 nanorod arrays with an area of 0.25 cm^2 served as working electrode. An Ag/AgCl (3 M KCl) and a platinum wire acted as reference electrode and counter electrode, respectively. The measurements were carried out on a Zennium electrochemical workstation and a controlled intensity modulated photo spectroscopy (CIMPS) system (Zahner, Germany) interfaced to an ultraviolet light emitting diode with maximum intensity of 3.8 mW cm^{-2} at wavelength of 365 nm. Linear sweeping voltammograms (LSVs) were performed at a scan rate of 5 mV s^{-1}, and all photocurrent responses and steady-state photocurrents were obtained under UV illumination of 2.0 mW cm^{-2}.

3. Results and discussion

3.1. Morphology and phase characterization of TiO_2 nanorod arrays

After oxidizing with the 30 wt% H_2O_2 solution for 72 h at 80 °C, the Ti foil had lost its metallic luster and turned grayish white, while white precipitations appeared in the solution. The color of the solution also changed slowly from colorless to yellow after the oxidation began, and then faded to colorless again at the end of the reaction. The color came from the formation of the complex $[TiO(H_2O_2)]^{2+}$ [37], and its disappearance resulted from the decomposition of the complex caused by forming TiO_2 precipitation with higher stability. Fig. 2A shows the typical images of as-prepared samples. Vertically oriented TiO_2 nanorods with high density have been uniformly formed on a large scale on the Ti substrate. These nanorods have diameters of 20–50 nm with lengths of 1.5 μm. Fig. 2B shows the image of TiO_2 nanorod arrays after thermal treatment at 500 °C, which indicates that the morphology of the samples didn't change and the expected nanoarrays shown in Fig. 1B for efficient electron transport were successfully constructed. Fig. 3 shows the XRD patterns of Ti foil and samples with and without thermal treatment at various temperatures. The TiO_2 nanorods had been crystallized prior to thermal treatment, and XRD patterns could be indexed to those of anatase. The sample was partially converted into rutile (13%) after thermal treatment at 300 °C. The rutile content gradually increased from 15% to 21% with the thermal treatment temperature rising from 400 °C to 500 °C. Finally, a mixture of anatase and rutile nanorods was finally formed.

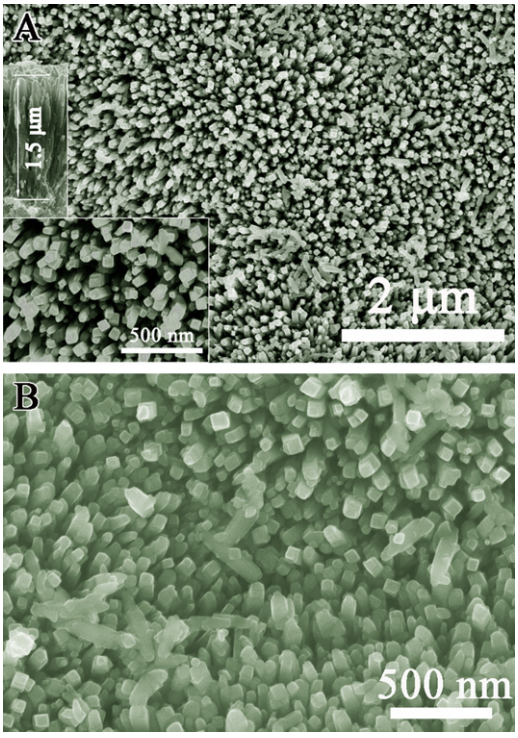

Fig. 2. (A) Typical images of as-prepared TiO_2 nanorods; inset is high magnification of TiO_2 nanorods. (B) TiO_2 nanorods after thermal treatment at 500 °C.

3.2. Photoelectrochemical characterization of TiO_2 nanorod arrays

The photoelectrochemical properties of the samples were evaluated by linear sweeping voltammograms performed under UV illumination of 2.0 mW cm^{-2} (Fig. 4A). The results showed that the photocurrent increased with the increased potential applied for each sample before leveling off to a saturated photocurrent. This suggests that the separation of the photogenerated electrons and holes is the rate-limiting step within the low potential region (−0.4 V to +0.1 V). The photocurrent leveled off at higher potentials (+0.1 V to +0.8 V) indicating that the charge separation was not the rate-limiting process any longer [38]. Higher responsive photocurrent means lower recombination of electrons and holes and higher photoelectron transfer efficiency for the TiO_2 nanorod arrays, which will eventually benefit the corresponding photoelectrocatalysis [39]. The saturated photocurrent of the anatase and rutile mixed crystal TiO_2 nanorod arrays was higher than that of anatase TiO_2 nanorod arrays. The higher photocurrent may be attributed to two aspects. One resulted from the complete crystallization brought by thermal treatment. High-temperature treatment usually improves the crystallinity of TiO_2 nanomaterials, but the process in turn can induce the aggregation of small nanoparticles [35]. The narrowing widths of the anatase diffraction peaks (Fig. 3) also demonstrate the grain growth. Other works confirmed the anatase TiO_2 after thermal treatment at 400–500 °C had a higher photoactivity, while the photoactivity decreased due to the sharp drop of the specific surface area after thermal treatment at higher temperature [30–42]. The other contribution to the higher photocurrent was ascribed to the mixed crystal effect because of the band match between anatase and rutile crystals. The photogenerated electrons on the conduction band (CB) of anatase could be injected to the CB of rutile nearby and the photogenerated holes on the valence band (VB) of rutile injected to the VB of anatase, which improved the charge separation and generated an improved photocurrent response [43]. All those effects resulted in the final fact that the increase of rutile content led to an increase in photocurrent, but the increasing rate was gradually depressed. Displayed in Fig. 4B are the photocurrent responses of TiO_2 nanorod arrays when applied potential biases were 0 V and +0.4 V, respectively. The rise and fall of the photocurrent corresponded well to the UV illumi-

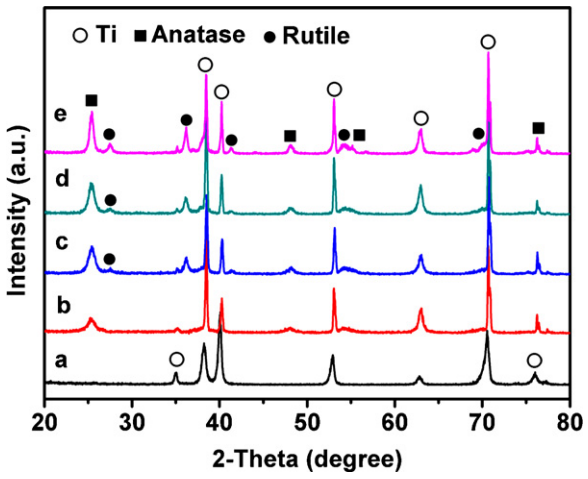

Fig. 3. XRD patterns of (a) Ti substrate, (b) as-prepared TiO_2 nanorods, and TiO_2 nanorods annealed at (c) 300 °C, (d) 400 °C, and (e) 500 °C.

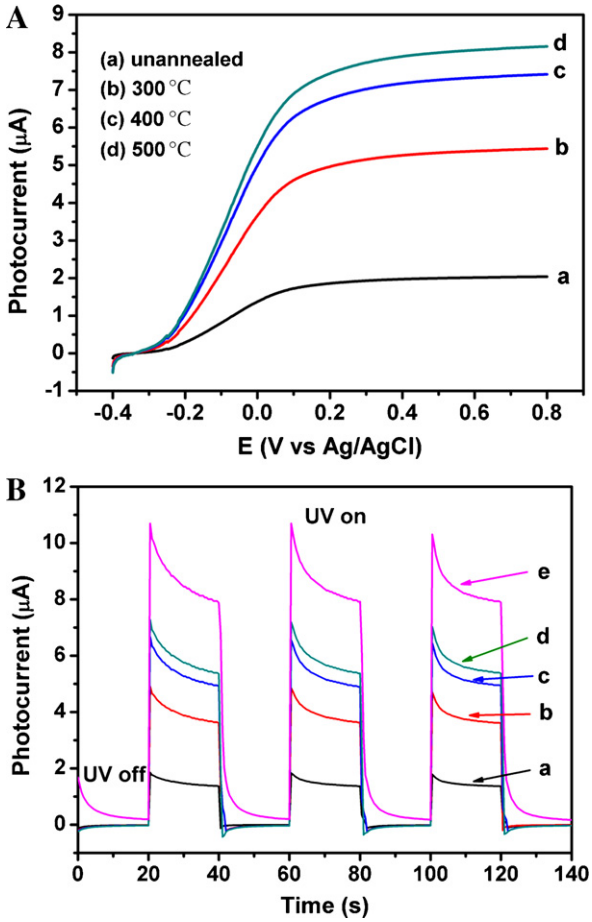

Fig. 4. (A) LSVs of (a) as-prepared TiO_2 nanorods, (b) TiO_2 nanorods annealed at 300 °C, (c) 400 °C and (d) 500 °C. (B) Photocurrent responses of (a) as-prepared TiO_2 nanorods, (b) TiO_2 nanorods annealed at 300 °C, (c) 400 °C and (d) 500 °C measured at a potential bias of 0 V, and (e) TiO_2 nanorods annealed at 500 °C measured at a potential bias of 0.4 V.

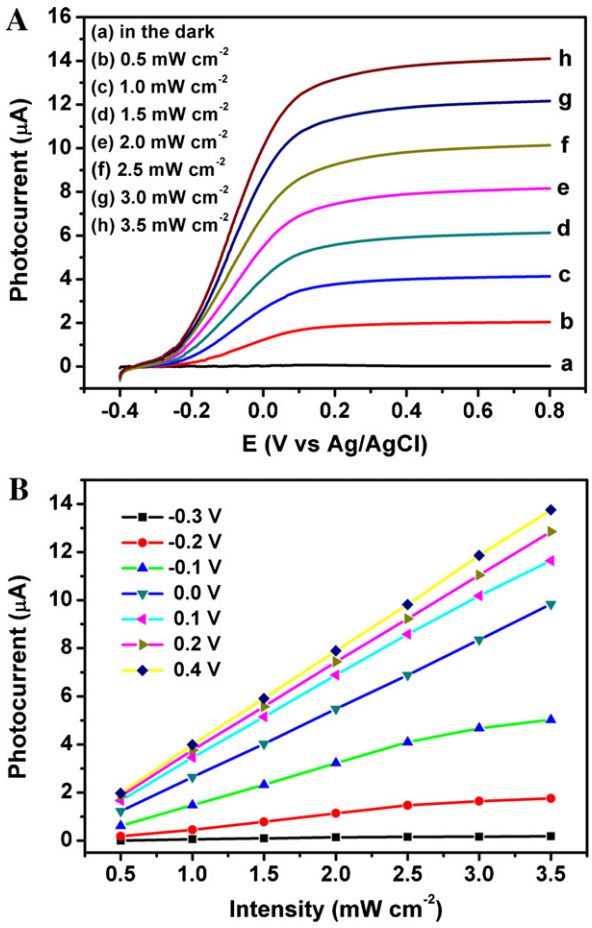

Fig. 5. (A) LSVs of TiO_2 nanorods annealed at 500 °C under UV illumination of various intensities. (B) The plots of photocurrent against UV illumination intensity using various potential biases.

nation being switched on and off for all the samples. The current responses in the dark were negligible, which meant that no electrochemical oxidation occurred. In the case of UV illumination, an apparently boosted photocurrent response appeared indicating the happening of photoelectrocatalysis. The sample with thermal treatment at 500 °C showed much higher photocurrent than the other samples, whereas the same increasing trend as that of the LSVs was observed. However, a significant increase could be obtained if the absent bias was replaced by +0.4 V. The stronger photocurrent is mainly due to the enhanced separation of electrons and holes benefited from the potential bias, and improved photocatalytic efficiency could be expected [44].

Fig. 5 presents the effect of illumination intensity on the photocurrent originated from the photocatalysis of TiO_2 nanorod arrays annealed at 500 °C. The saturated photocurrent increased regularly if linearly increased illumination intensity was applied (Fig. 5A). Fig. 5B derived from Fig. 5A shows the dependence of photocurrent on the illumination intensity when using various potential biases. A linear relationship was observed if the potential bias was over 0, but the linearity did not remain good when the applied potential bias was negative. The photocurrents were on the low side because the photoelectrons were not fully transported to external circuit by lower biases. The higher the intensity the more positive potential is needed for effective charge separation. It can be drawn from the above that the photoelectrons transported are proportional to light intensity as long as the applied potential bias is positive enough [45]. Therefore, a constant potential bias of +0.4 V was used for the following experiments to maximize the photocatalytic efficiency.

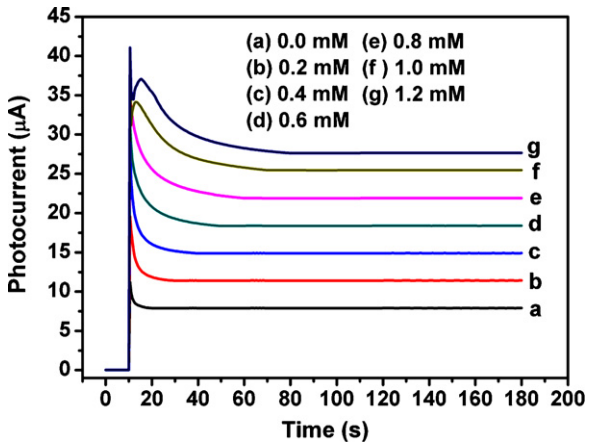

Fig. 6. Photocurrent responses of TiO_2 nanorod arrays annealed at 500 °C to various concentrations of glucose.

3.3. Photoelectrochemical performance for organics-sensing application

The above investigations demonstrated that the sample with thermal treatment at 500 °C had the best photoelectrocatalytic activities among the four samples. The sample was therefore used to oxidize various organic matters in order to verify its suitability for organics-sensing application. Fig. 6 shows the photocurrent of the 500 °C thermally treated sample measured in the photoelectrochemical cell containing solutions with various concentrations of glucose. The dark currents are almost zero without UV illumination for all glucose concentrations, which indicates that glucose was not electrocatalytically oxidized, although a potential bias of +0.4 V had been applied on the TiO_2 nanorod arrays electrode. Under UV illumination, a tremendous increase in current instantaneously appeared due to the preadsorption of water and glucose on the electrode [46]. The photocurrent decayed once the current reached its peak, and a steady state of the current (denoted as i_{ss}) was subsequently achieved. Moreover, an increasing tend of i_{ss} with the increased concentration of glucose could be seen. For the solution without glucose, the steady-state photocurrent (denoted as i_{blank}) mainly resulted from the oxidation of water, while i_{ss} was composed of two different components, one resulting from the oxidation of organics and the other from the oxidation of water [28]. The net steady-state current i_{net} originated from the oxidation of the organics can be obtained by subtracting i_{blank} from i_{ss} in the presence of organic compounds: $i_{net} = i_{ss} - i_{blank}$. i_{net} can be used to quantify the concentration of the organic compounds in aqueous solutions, because the mass transport of organics to the electrode surface within a certain range of concentrations was a limiting step in the photoelectrocatalytic oxidation process [46].

Fig. 7 shows the relationship between the glucose concentrations and the i_{net} values. For all the investigated samples, i_{net} increased as the glucose concentration increased, while different linear range was obtained. The sample with thermal treatment at 500 °C exhibited the most excellent performance which had the widest linear range with an upper limit of 1.1 mM. In comparison, upper limits of 0.9 mM and 0.7 mM could be achieved by the samples annealed at 400 °C and 300 °C, respectively. For the sample without thermal treatment, i_{net} gradually deviated from the straight line when glucose concentration only reached 0.5 mM. The lower upper limit was due to the inefficient photocatalysis which depressed the oxidation of glucose. As a result, the photocatalysis took the place of mass transport and gradually became the limiting step as the glucose concentration increased. These results conform

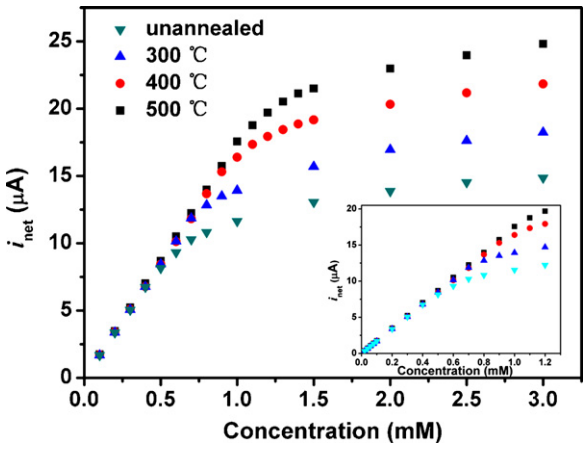

Fig. 7. The plots of i_{net} value against glucose concentration for each sample.

to the aforementioned observation in the photoelectrochemical characterization of the samples.

For the determination of other organics, the sample with best performance was used to carry out photocatalysis in order to demonstrate its sensibility to organic compounds in aqueous solutions. Fig. 8A shows the relationship between the i_{net} values and the concentrations of various organics. It was found that the i_{net} was directly proportional to the concentration for all the investigated organic compounds. Photocatalysis is actually a process which photogenerated holes capture electrons from organic compounds.

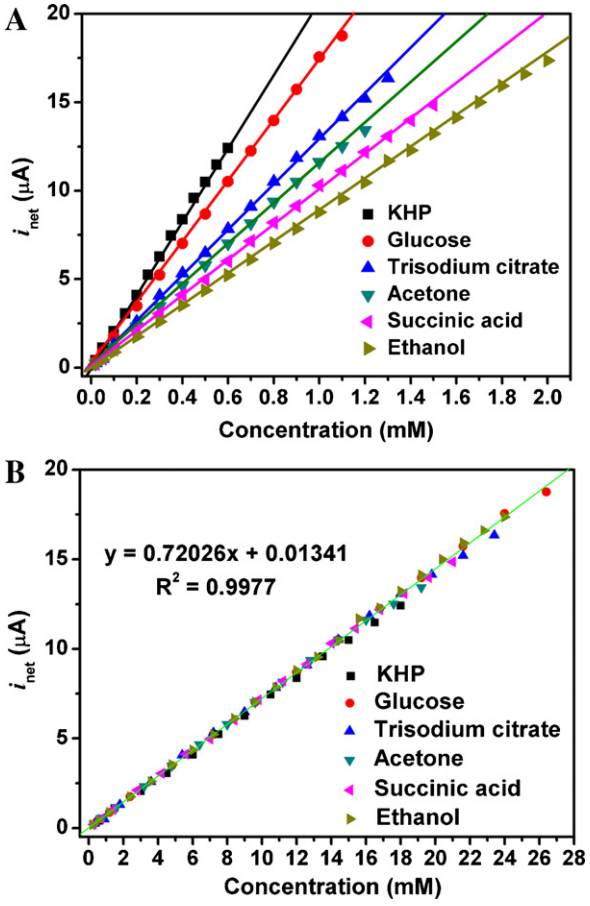

Fig. 8. (A) The plots of i_{net} values against concentrations of various organics. (B) The plot of i_{net} value against concentration of electrons transferred in exhaustive oxidation for various organics.

Table 1
The number of transferred electrons (n) in exhaustive oxidation for the investigated organic compounds.

Organic compounds	Molecular structure	n
Ethanol	CH_3CH_2OH	12
Succinic acid	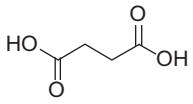	14
Acetone		16
Trisodium citrate	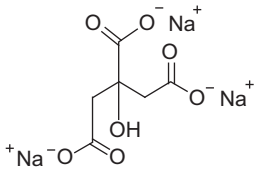	18
Glucose	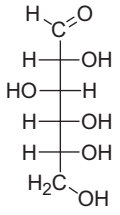	24
Potassium hydrogen phthalate (KHP)	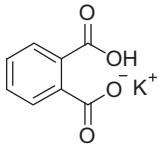	30

Different organic compounds will contribute different number of electrons when exhaustively oxidized into H_2O and CO_2. The number of electrons (n) transferred in exhaustive oxidation for the selected organic compounds are listed in Table 1. The concentration of these electrons can be obtained through multiplying the concentration of the organics by the number of transferred electrons (n). Then, a new relationship for the i_{net} was established by replacing the concentration of organics with the concentration of transferred electrons, as shown in Fig. 8B. Excellent linearity (R^2 = 0.9977) between the i_{net} and the concentration of transferred electrons was obtained. The detection limit was 0.2 mM for the transferred electrons based on three times the standard deviation (S/N = 3) of the blank solution with 11 parallel measurements. Consequently, the detection limit for each organic compound could be obtained by dividing 0.2 mM by the corresponding number of transferred electrons. For example, the detection limits were 8 μM and 14 μM for glucose and succinic acid, respectively. Moreover, the prepared TiO_2 nanorod arrays had good adhesion to the Ti substrate, and did not easily lifted off in continuous operations, which resulted in an excellent reproducibility in determination of organics. The relative standard deviation was 1.32% for 0.5 mM glucose at 10 repetitive measurements. These results suggest a potential application of the TiO_2 nanorod arrays as a sensor not only for individual organic compound but for a group of organic compounds.

4. Conclusion

The present paper demonstrated high-density arrays of vertically oriented TiO_2 nanorods on Ti foil by a simple and undefiled method via oxidizing Ti foil in H_2O_2 solution. This method was template-free, and the formed TiO_2 nanorod arrays were in anatase

phase prior to thermal treatment or mixed phase after thermal treatment. The photoelectrochemical experiments indicated that the TiO_2 nanorod arrays in mixed phase presented higher photocatalytic activity than the anatase TiO_2 nanorod arrays. Sensing ability for organics in aqueous solutions by steady-state photocurrent resulted from photocatalysis of TiO_2 nanorod was exhibited. The i_{net} was directly proportional to the concentration for all the investigated organic compounds. The mixed crystal TiO_2 nanorod arrays which had the highest photocurrent exhibited the best performance in determination of organics in aqueous solution.

Acknowledgements

We gratefully acknowledge the financial support of Shanghai Municipal Education Commission (no. 07SG37), National Natural Science Foundation of China (no. 51072034), Shanghai Leading Academic Discipline Project (B603), the Cultivation Fund of the Key Scientific and Technical Innovation Project (no. 708039), and the Program of Introducing Talents of Discipline to Universities (no. 111-2-04).

References

[1] J. Wu, C. Yu, Aligned TiO_2 nanorods and nanowalls, J. Phys. Chem. B 108 (2004) 3377–3379.
[2] D. Daniel, I.G.R. Gutz, Microfluidic cell with a TiO_2-modified gold electrode irradiated by an UV-LED for in situ photocatalytic decomposition of organic matter and its potentiality for voltammetric analysis of metal ions, Electrochem. Commun. 9 (2007) 522–528.
[3] T. Yang, C. Shiu, M. Wong, Structure and hydrophilicity of titanium oxide films prepared by electron beam evaporation, Surf. Sci. 548 (2004) 75–82.
[4] H. Sun, C. Wang, S. Pang, X. Li, Y. Tao, H. Tang, Photocatalytic TiO_2 films prepared by chemical vapor deposition at atmosphere pressure, J. Non-Cryst. Solids 354 (2008) 1440–1443.
[5] A. Sobczyk-Guzenda, M. Gazicki-Lipman, H. Szymanowski, J. Kowalski, P. Wojciechowski, T. Halamus, A. Tracz, Characterization of thin TiO_2 films prepared by plasma enhanced chemical vapour deposition for optical and photocatalytic applications, Thin Solid Films 517 (2009) 5409–5414.
[6] C. Giolli, F. Borgioli, A. Credi, A.D. Fabio, A. Fossati, M.M. Miranda, S. Parmeggiani, G. Rizzi, A. Scrivani, S. Troglio, A. Tolstoguzov, A. Zoppi, U. Bardi, Characterization of TiO_2 coatings prepared by a modified electric arc-physical vapour deposition system, Surf. Coat. Technol. 202 (2007) 13–22.
[7] K.K. Saini, S.D. Sharma, M.K. Chanderkant, D. Singh, C.P. Sharma, Structural and optical properties of TiO_2 thin films derived by sol–gel dip coating process, J. Non-Cryst. Solids 353 (2007) 2469–2473.
[8] S. Sokolov, E. Ortel, J. Radnik, R. Kraehnert, Influence of steel composition and pre-treatment conditions on morphology and microstructure of TiO_2 mesoporous layers produced by dip coating on steel substrates, Thin Solid Films 518 (2009) 27–35.
[9] E.M. El-Maghraby, Y. Nakamura, S. Rengakuji, Composite TiO_2–SnO_2 nanostructured films prepared by spin-coating with high photocatalytic performance, Catal. Commun. 9 (2008) 2357–2360.
[10] P.S. Marcos, J. Marto, T. Trindade, J.A. Labrincha, Screen-printing of TiO_2 photocatalytic layers on glazed ceramic tiles, J. Photochem. Photobiol. A 197 (2008) 125–131.
[11] K. Fan, M. Liu, T. Peng, L. Ma, K. Dai, Effects of paste components on the properties of screen-printed porous TiO_2 film for dye-sensitized solar cells, Renew. Energy 35 (2010) 555–561.
[12] H. Yu, S. Zhang, H. Zhao, B. Xue, P. Liu, G. Will, High-performance TiO_2 photoanode with an efficient electron transport network for dye-sensitized solar cells, J. Phys. Chem. C 113 (2009) 16277–16282.
[13] G.K. Mor, K. Shankar, M. Paulose, P.K. Varghese, C.A. Grimes, Use of highly-ordered TiO_2 nanotube arrays in dye-sensitized solar cells, Nano Lett. 6 (2006) 215–218.
[14] Q. Zeng, L. Wu, Y. Zhang, B. Qi, J. Zhi, Low-temperature and normal-pressure growth of oriented rutile TiO_2 nanorod arrays on F-doped tin oxide substrate, Scripta Mater. 62 (2010) 810–813.
[15] D. Wang, Y. Liu, B. Yu, F. Zhou, W. Liu, TiO_2 nanotubes with tunable morphology, diameter, and length: synthesis and photo-electrical/catalytic performance, Chem. Mater. 21 (2009) 1198–1206.
[16] Z. Liu, B. Pesic, K.S. Raja, R.R. Rangaraju, M. Misra, Hydrogen generation under sunlight by self ordered TiO_2 nanotube arrays, Int. J. Hydrogen Energy 34 (2009) 3250–3257.
[17] K.Y. Cheung, C.T. Yip, A.B. Djurišic, Y.H. Leung, W.K. Chan, Long K-doped titania and titanate nanowires on Ti foil and fluorine-doped tin oxide/quartz substrates for solar-cell applications, Adv. Funct. Mater. 17 (2007) 555–562.
[18] X. Feng, K. Shankar, O.K. Varghese, M. Paulose, T.J. Latempa, C.A. Grimes, Vertically aligned single crystal TiO_2 nanowire arrays grown directly on transparent conducting oxide coated glass: synthesis details and applications, Nano Lett. 8 (2008) 3781–3786.
[19] Y. Li, T. Sasaki, Y. Shimizu, N. Koshizaki, Hexagonal-close-packed, hierarchical amorphous TiO_2 nanocolumn arrays: transferability, enhanced photocatalytic activity, and superamphiphilicity without UV irradiation, J. Am. Chem. Soc. 130 (2008) 14755–14762.
[20] J. Qiu, Z. Jin, Z. Liu, X. Liu, G. Liu, W. Wu, X. Zhang, X. Gao, Fabrication of TiO_2 nanotube film by well-aligned ZnO nanorod array film and sol–gel process, Thin Solid Films 515 (2007) 2897–2902.
[21] J. Lee, I. Leu, M. Hsu, Y. Chung, M. Hon, Fabrication of aligned TiO_2 one-dimensional nanostructured arrays using a one-step templating solution approach, J. Phys. Chem. B 109 (2005) 13056–13059.
[22] X. Peng, A. Chen, Aligned TiO_2 nanorod arrays synthesized by oxidizing titanium with acetone, J. Mater. Chem. 14 (2004) 2542–2548.
[23] X. Peng, J. Wang, D.F. Thomas, A. Chen, Tunable growth of TiO_2 nanostructures on Ti substrates, Nanotechnology 16 (2005) 2389–2395.
[24] B. Liu, E.S. Aydil, Growth of oriented single-crystalline rutile TiO_2 nanorods on transparent conducting substrates for dye-sensitized solar cells, J. Am. Chem. Soc. 131 (2009) 3985–3990.
[25] S. Li, G. Ye, G. Chen, Low-temperature preparation and characterization of nanocrystalline anatase TiO_2, J. Phys. Chem. C 113 (2009) 4031–4037.
[26] I.R. Bickler, T. Gonzalez-Carreno, J.S. Lees, L. Palmisano, R.J.D. Tilleyd, A structural investigation of titanium dioxide photocatalysts, J. Solid State Chem. 92 (1991) 178–180.
[27] C. Sun, N. Wang, S. Zhou, X. Hu, S. Zhou, P. Chen, Preparation of self-supporting hierarchical nanostructured anatase/rutile composite TiO_2 film, Chem. Commun. (2008) 3293–3295.
[28] S. Zhang, L. Li, H. Zhao, A portable photoelectrochemical probe for rapid determination of chemical oxygen demand in wastewaters, Environ. Sci. Technol. 43 (2009) 7810–7815.
[29] S. Ai, M. Gao, Y. Yang, J. Li, L. Jin, Electrocatalytic sensor for the determination of chemical oxygen demand using a lead dioxide modified electrode, Electroanalysis 16 (2004) 404–409.
[30] J. Li, L. Li, L. Zheng, Y. Xian, L. Jin, Rh_2O_3/Ti electrode preparation using laser anneal and its application to the determination of chemical oxygen demand, Meas. Sci. Technol. 17 (2006) 1995–2000.
[31] K. Lee, T. Ishikawa, S.J. McNiven, Y. Nomura, A. Hiratsuka, S. Sasaki, Y. Arikawa, I. Karube, Evaluation of chemical oxygen demand (COD) based on coulometric determination of electrochemical oxygen demand (EOD) using a surface oxidized copper electrode, Anal. Chim. Acta 398 (1999) 161–171.
[32] C.R. Silva, C.D.C. Conceição, V.G. Bonifácio, O.F. Filho, M.F.S. Teixeira, Determination of the chemical oxygen demand (COD) using a copper electrode: a clean alternative method, J. Solid State Electrochem. 13 (2009) 665–669.
[33] H. Yu, H. Wang, X. Quan, S. Chen, Y. Zhang, Amperometric determination of chemical oxygen demand using boron-doped diamond (BDD) sensor, Electrochem. Commun. 9 (2007) 2280–2285.
[34] H. Yu, C. Ma, X. Quan, S. Chen, H. Zhao, Flow injection analysis of chemical oxygen demand (COD) by using a boron-doped diamond (BDD) electrode, Environ. Sci. Technol. 43 (2009) 1935–1939.
[35] X. Chen, S.S. Mao, Titanium dioxide nanomaterials: synthesis, properties, modifications, and applications, Chem. Rev. 107 (2007) 2891–2959.
[36] R.A. Spurr, H. Myers, Quantitative analysis of anatase-rutile mixtures with an X-ray diffractometer, Anal. Chem. 29 (1957) 760–762.
[37] X. Wei, Y. Zhang, Z. Jiang, A. Liang, A simple and sensitive SPRS method for trace H_2O_2 based on the TiO^{2+} complex and gold nanoparticles aggregation reactions, Plasmonics 4 (2009) 181–185.
[38] Z. Zhang, Y. Yuan, L. Liang, Y. Cheng, G. Shi, L. Jin, Preparation and photoelectrocatalytic activity of ZnO nanorods embedded in highly ordered TiO_2 nanotube arrays electrode for azo dye degradation, J. Hazard. Mater. 158 (2008) 517–522.
[39] Y. Xie, Photoelectrochemical reactivity of a hybrid electrode composed of polyoxophosphotungstate encapsulated in titania nanotubes, Adv. Funct. Mater. 16 (2006) 1823–1831.
[40] T. Peng, D. Zhao, K. Dai, W. Shi, K. Hirao, Synthesis of titanium dioxide nanoparticles with mesoporous anatase wall and high photocatalytic activity, J. Phys. Chem. B 109 (2005) 4947–4952.
[41] J. Yu, X. Zhao, Q. Zhao, Effect of surface structure on photocatalytic activity of TiO_2 thin films prepared by sol–gel method, Thin Solid Films 379 (2000) 7–14.
[42] G. Yang, C. Li, F. Han, X. Huang, Effects of annealing treatment on microstructure and photocatalytic performance of nanostructured TiO_2 coatings through flame spraying with liquid feedstocks, J. Vac. Sci. Technol. B 22 (2004) 2364–2368.
[43] R.I. Bickley, T. Gonzalez-Carreno, J.S. Lees, L. Palmisano, R.J.D. Tilley, A structural investigation of titanium dioxide photocatalysts, J. Solid State Chem. 92 (1991) 178–190.
[44] G. Zhang, H. Huang, Y. Zhang, H.L.W. Chan, L. Zhou, Highly ordered nanoporous TiO_2 and its photocatalytic properties, Electrochem. Commun. 9 (2007) 2854–2858.
[45] D. Jiang, H. Zhao, Z. Jia, Photoelectrochemical behaviour of methanol oxidation at nanoporous TiO_2 film electrodes, J. Photochem. Photobiol. A 144 (2001) 197–204.
[46] Y. Han, S. Zhang, H. Zhao, W. Wen, H. Zhang, H. Wang, F. Peng, Photoelectrochemical characterization of a robust TiO_2/BDD heterojunction electrode for sensing application in aqueous solutions, Langmuir 26 (2010) 6033–6040.